applied optics

Amplitude versus phase effects in extreme ultraviolet lithography mask scattering and imaging

Patrick P. Naulleau,[1,*] Markus Benk,[1] Kenneth A. Goldberg,[1] Eric M. Gullikson,[1] Antoine Wojdyla,[1] Yow-Gwo Wang,[2] and Andy Neureuther[2]

[1]Center for X-Ray Optics, Lawrence Berkeley National Laboratory, Berkeley, California 94720, USA
[2]University of California at Berkeley, Berkeley, California 94720, USA
*Corresponding author: PNaulleau@lbl.gov

Received 23 December 2016; revised 11 March 2017; accepted 15 March 2017; posted 15 March 2017 (Doc. ID 283458); published 13 April 2017

It is now well established that extreme ultraviolet (EUV) mask multilayer roughness leads to wafer-plane line-width roughness (LWR) in the lithography process. Analysis and modeling done to date has assumed, however, that the roughness leading to scatter is primarily a phase effect and that the amplitude can be ignored. Under this assumption, simple scattering measurements can be used to characterize the statistical properties of the mask roughness. Here, we explore the implications of this simplifying assumption by modeling the imaging impacts of the roughness amplitude component as a function of the balance between amplitude and phase induced scatter. In addition to model-based analysis, we also use an EUV microscope to compare experimental through focus data to modeling in order to assess the actual amount of amplitude roughness on a typical EUV multilayer mask. The results indicate that amplitude roughness accounts for less than 1% of the total scatter for typical EUV masks.

OCIS codes: (110.5220) Photolithography; (120.3940) Metrology; (260.7200) Ultraviolet, extreme; (340.7480) X-rays, soft x-rays, extreme ultraviolet (EUV).

https://doi.org/10.1364/AO.56.003325

1. INTRODUCTION

Extreme ultraviolet (EUV) lithography, being a short wavelength technique based on reflective optics and masks, is highly susceptible to roughness. When this roughness is present on the mask, it has been shown to lead to image plane speckle and, ultimately, line-width roughness (LWR) in the imaging process [1–4]. Analysis and modeling done to date has assumed that the roughness leading to scatter is primarily a phase effect and that the amplitude (or local variations in the reflectivity) can be ignored [1]. Under this assumption, simple angle resolved scattering measurements can be used to characterize the statistical properties of the mask roughness [5]. Here, we explore the implications of this simplifying assumption by modeling the imaging impacts of the roughness amplitude component as a function of the balance between amplitude and phase induced scatter. The results show the imaging characteristics to be dramatically different between phase and amplitude roughness. Thus, determining the magnitude of the amplitude roughness term is critical. To this end, we compare modeled through focus clear field speckle images to experimental results obtained using a synchrotron-based EUV mask microscope [6].

2. MEASURING EUV ROUGHNESS

EUV lithography masks [7] are comprised of multilayer [8] coated plates with a capping layer and a patterned absorber on top (Fig. 1). The roughness with which we are concerned here is that within the multilayer reflector impacting the reflected wavefront. With roughness, a random phase term (and possibly a random amplitude term) is added to the wavefront upon reflection, causing deviations from the specular reflection, or scatter. The typical method used to measure the mask multilayer roughness is with atomic force microscopy (AFM). With this method, we must assume that the measured top surface roughness is in fact replicated throughout the Bragg structure. This assumption is known as the *single surface approximation* [9] and leads to a direct mapping between the measured surface roughness and reflected phase, but has zero impact on the reflected amplitude. In addition to the pure phase limitation, the AFM approach is susceptible to errors arising from the top surface roughness not, in fact, matching the Bragg structure roughness, as shown in Fig. 1, where the capping layer roughness is different than the Bragg structure roughness. The limitations of

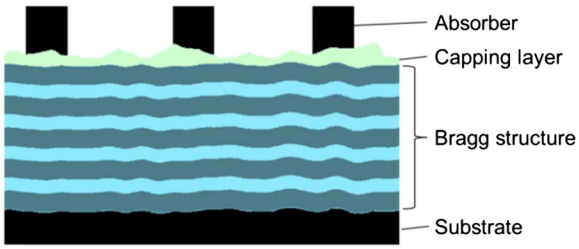

Fig. 1. Schematic of EUV mask structure with roughness.

the AFM approach have been documented in the literature [10].

As discussed above, the impact of the roughness is to scatter light with the angle being proportional to the frequency of the roughness, thus, scatter angle resolved scattering measurements can also be used to determine the roughness. The benefit of this approach is that it can be done using EUV light in which case the true Bragg structure roughness of interest can be determined. Given the fact that EUV lithography masks are required to be very smooth relative to the EUV wavelength, the structure roughness can be determined using the Rayleigh–Rice model [11], whereby the roughness power spectral density (PSD) is expressed as

$$\mathrm{PSD}(\theta_s) = \frac{R(\theta_s)\lambda^4}{16\pi^2 \cos(\theta_i)\cos(\theta_s)R_o}, \tag{1}$$

where $R(\theta_s)$ is the reflectivity as a function of scattering angle, θ_s is the scattering angle, θ_i is the incidence angle, and R_o is the zero roughness reflectivity limit of the Bragg structure. Note that the Rayleigh–Rice model assumes that all the scattering arises from small phase perturbations. As with the single surface approximation, this leads to a pure phase roughness surface or no amplitude roughness (local reflectivity variations). The small phase approximation also leads to an ambiguity between phase and amplitude in that the scattering produced by small phase perturbations becomes indistinguishable from that produced by small amplitude perturbations, namely,

$$|\Im(1+a)| \sim |\Im(e^{ja})|, \tag{2}$$

where $\Im$ represents the Fourier transform, or far field diffraction, from the surface. This ambiguity is depicted in Fig. 2,

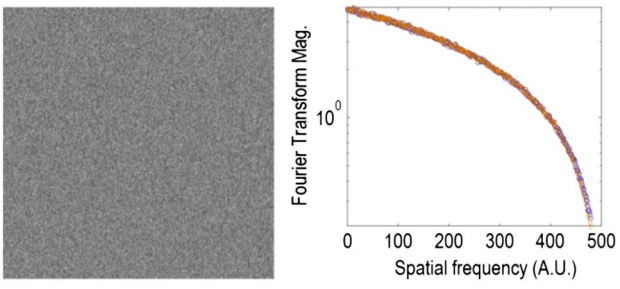

Fig. 2. Surface distribution (left) and the isotropic Fourier transform magnitude of the surface (right), assuming the surface to be either a phase $\exp(ja)$ (blue circle markers) or amplitude $(1+a)$ (orange diamond markers) disturbance, respectively. In the computation, a is a Gaussian random variable with a standard deviation of 0.1.

which shows a surface distribution (left) and the isotropic Fourier transform magnitude of the surface (right), assuming the surface to be either a phase $\exp(ja)$ or amplitude $(1+a)$ disturbance, respectively, where a is a Gaussian random variable with a standard deviation of 0.1. The observed spectra are indistinguishable.

3. PHASE VERSUS AMPLITUDE ROUGHNESS

In the previous section, we showed that conventional roughness measurement techniques cannot distinguish between phase and amplitude roughness. Next, we consider how these different roughness types impact the imaging in terms of creating image plane speckle, which ultimately leads to LWR. The link between image speckle and LWR has been well described in the literature [1–4] but can be simply explained from the perspective of exposure latitude. By noting that speckle represents localized intensity variations, these variations translate to localized exposure dose variations and, thus, localized critical dimension (CD) changes, or LWR.

For the modeling, we use thin mask scalar aerial image computation software based on the partially coherent image formation equations [12]. It has previously been shown that in the case of EUV speckle modeling, the thin mask model is a suitable approximation to rigorous three-dimensional (3D) electromagnetic modeling [13]. The roughness standard deviation is assumed to be 68 pm with a peak to valley height of 650 pm. This value was taken from a high quality EUV mask, and the modeled roughness PSD is set to match that of typical EUV masks, having a correlation length of approximately 30 nm. For the imaging configuration, we assume an ideal 0.33 numerical aperture four times magnification EUV system and an illumination partial coherence of 0.5. We model a 500 nm × 500 nm clear area in the wafer plane (2000 nm × 2000 nm in the mask plane) and determine the standard deviation of the intensity (speckle) as a function of mask plane defocus. We define the speckle root mean squared (RMS) contrast as the ratio of the image intensity standard deviation and the image intensity mean. To the first order, if one knows the exposure latitude

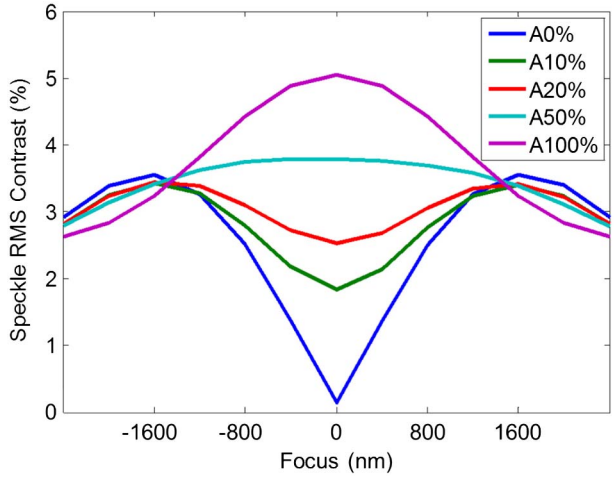

Fig. 3. Clear field speckle RMS contrast as a function of mask plane defocus and amplitude scattering content. $A0\%$ = pure phase roughness, and $A100\%$ = pure amplitude roughness.

for the patterning process of interest, one can use the speckle RMS contrast to get a rough estimate for the expected LWR. For example, if the 10% CD change exposure latitude is 20%, a speckle RMS contrast of 5% would lead to an estimated LWR of 2.5% of the CD, so for a CD of 20 nm, that would be a 0.5 nm LWR.

The speckle contrast modeling results are shown in Fig. 3 for five different realizations of roughness, all producing identical scattering power spectra, but being comprised of different ratios of amplitude and phase induced scatter, ranging from 0% amplitude content (A0%) to 100% amplitude content (A100%). It is evident that the imaging impact varies drastically as a function of amplitude content despite the scattering PSDs being identical in all cases.

4. MICROSCOPY-BASED ROUGHNESS MEASUREMENT

The above results demonstrate the image plane speckle properties to be highly dependent on the relative magnitudes of amplitude and phase contributions to the light scattered from the mask. Thus, an accurate assessment of mask roughness induced LWR contributions demands an accurate determination of the mask roughness amplitude content. However, such a measurement cannot be provided by scatterometry or AFM. To assess the relative importance of amplitude induced scatter on conventional EUV masks, we employ a synchrotron-based EUV mask microscope [6]. For the subsequent measurements, we use an effective numerical aperture of 0.33. The real numerical aperture is 0.0825 given that the EUV mask is intended for use in a four times magnification system. We also use an illumination partial coherence setting of 0.7.

Figure 4 shows images of the clear mask taken at three different focus settings, respectively. Note that the absolute contrast in the image set has been enhanced for visualization. The speckle contrast is seen to increase as a function of defocus as one would expect for a phase roughness dominate case.

Determination of the amplitude roughness content from these images relies in large part on the ability to measure the minimum contrast with high accuracy. To do so, we must

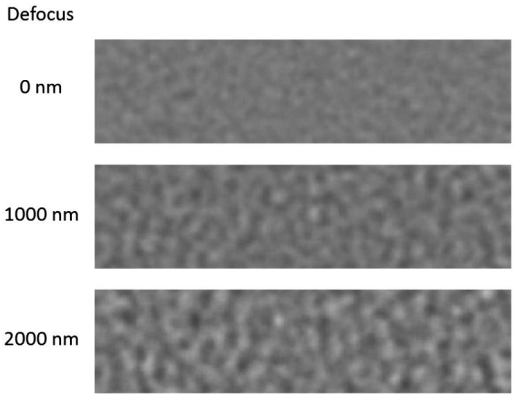

Fig. 4. Clear field speckle images from an EUV mask recorded using an EUV microscope with a mask plane numerical aperture of 0.0825 and a partial coherence of 0.7. Each image is taken at a different defocus value with the top image at 0 nm, the middle image at 1000 nm, and the bottom image at 2000 nm.

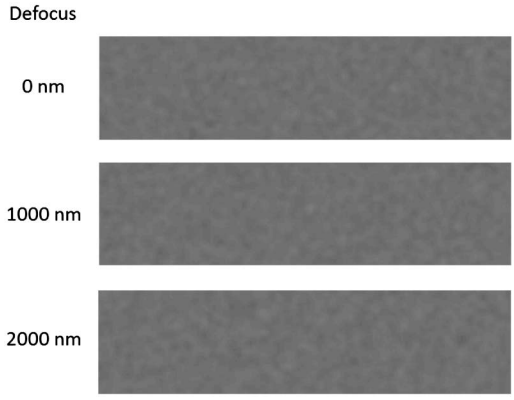

Fig. 5. Images used to determine the system noise floor. Imaging conditions are identical to those in Fig. 4 except that the mask is scanned through a length of more than 10,000 times greater than the roughness correlation length during the exposure. Each image is taken at a different defocus value. The measured RMS speckle contrast, and thus the noise floor, is 1.8%.

first determine the noise floor of the measurement and, thus, the speckle one would measure given an absolutely perfect mask. Since the masks we are measuring already represent the highest quality EUV masks, physically measuring such a reference to determine the noise floor is not possible. To overcome this limitation, we instead image the same mask while scanning the mask to wash out all mask contributions to the speckle. In this case, we keep the absolute exposure time the same as for the real measurement, thereby ensuring that the average exposure level, and thus the photon noise contribution to speckle, remains the same. We also choose the scan length to be more than 10,000 times greater than the roughness correlation length, thereby theoretically reducing the mask contributions by a factor of 100. Figure 5 shows the resulting images at the same three defocus values. In this case, as expected, we see no focus dependence, indicating that we have successfully removed the mask contributions and are measuring the system noise floor. The measured RMS speckle contrast is 1.8% in all cases.

5. AMPLITUDE ROUGHNESS CONTENT ON EUV MASKS

Using the EUV microscope method described above along with compensation for the noise floor, we determine through focus speckle behavior three different EUV mask blanks. The EUV reflectometry characterized roughness for the three masks was 106 pm, 80 pm, and 59 pm, for Masks 1 through 3, respectively. Figure 6 (solid lines) shows the noise-corrected measurement results with an illumination partial coherence of 0.7.

To determine the potential amplitude content in the EUV reflectometry measured values, we model the EUV microscope image formation as a function of mask roughness amplitude content. The imaging model includes the known aberration characteristics of the microscope, including conventional aberrations as well as focal tilt across the field of view [14] and chromatic effects arising from the diffractive lens. The diamond shaped markers in Fig. 6 show the model results assuming

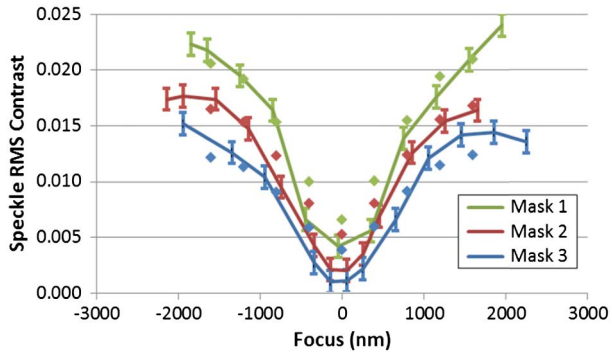

Fig. 6. Solid lines with error bars show measured EUV speckle contrast through focus (mask plane) after quadrature subtraction of noise floor. Diamond markers show modeled results assuming 1% amplitude roughness content. Results shown for three different masks; the EUV reflectometry characterized roughness for the three masks was 106 pm, 80 pm, and 59 pm, respectively.

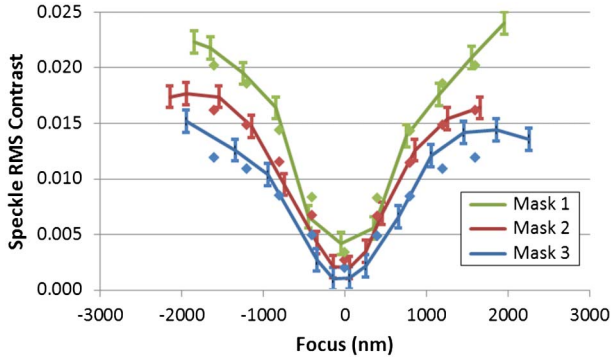

Fig. 7. Solid lines with error bars show measured EUV speckle contrast through focus (mask plane) after quadrature subtraction of noise floor. Diamond markers show modeled results assuming pure phase roughness.

an amplitude content of 1%. We see that at even this small level of amplitude content, significant discrepancies exist near the focus, whereas better agreement is seen at large defocus values.

Repeating the comparison from Fig. 6, but instead assuming pure phase roughness, yields the results shown in Fig. 7. Here, we see better agreement, indicating that typical EUV mask roughness can indeed be assumed to be pure phase. To quantify the relative quality of the two fits, we compute the square root of the sum of squared fractional errors for the two cases. The first case (assuming 1% amplitude content) yields an error metric of 4.12, whereas the second case (assuming pure phase roughness) yields an error metric of 1.67, confirming the significantly better fit.

6. SUMMARY

Modeling has shown the imaging impact of EUV mask roughness to be highly sensitive to the source of scatter: either random phase variations or random reflectivity (amplitude) variations in the reflected field. EUV scatterometry, however, cannot distinguish between these two sources of scatter, putting into question the validity of the technique for the characterization of EUV mask roughness. Direct comparison of aerial image modeling results to EUV microscopy imaging of EUV mask blanks with a range of roughness values, however, has shown that real EUV masks suffer from negligible amounts of amplitude roughness thereby allowing the pure phase approximation to be used, and consequently validating EUV scatterometry as an accurate EUV mask roughness characterization method.

Funding. Intel Corporation (DE-AC02-05CH11231).

Acknowledgment. This work was supported by Intel through the U.S. Department of Energy under Contract No. DE-AC02-05CH11231.

REFERENCES

1. P. Naulleau, "The relevance of mask-roughness-induced printed line-edge roughness in recent and future EUV lithography tests," Appl. Opt. **43**, 4025–4032 (2004).
2. P. Naulleau, "Correlation method for the measure of mask-induced line-edge roughness in extreme ultraviolet lithography," Appl. Opt. **48**, 3302–3307 (2009).
3. P. Naulleau and S. George, "Implications of image plane line-edge roughness requirements on extreme ultraviolet mask specifications," Proc. SPIE **7379**, 73790O (2009).
4. E. Gallagher, G. McIntyre, T. Wallow, S. Raghunathan, O. Wood, L. Kindt, J. Whang, and M. Barrett, "EUV masks under exposure: practical considerations," Proc. SPIE **7969**, 79690W (2011).
5. R. Chao, E. Gullikson, M. Goldstein, F. Goodwin, R. Teki, A. Neureuther, and P. Naulleau, "EUV scatterometry-based measurement method for the determination of phase roughness," Proc. SPIE **8880**, 88801B (2013).
6. K. Goldberg, I. Mochi, M. Benk, C. Lin, A. Allezy, M. Dickinson, C. Cork, J. Macdougall, E. Anderson, W. Chao, F. Salmassi, E. Gullikson, D. Zehm, V. Vytla, W. Cork, J. DePonte, G. Picchi, A. Pekedis, T. Katayanagi, M. Jones, E. Martin, P. Naulleau, and S. Rekawa, "The SEMATECH high-NA actinic reticle review project (SHARP) EUV mask-imaging microscope," Proc. SPIE **8880**, 88800T (2013).
7. S. Hector, "EUVL masks: requirements and potential solutions," Proc. SPIE **4688**, 134–149 (2002).
8. J. H. Underwood and T. W. Barbee, Jr., "Layered synthetic microstructures as Bragg diffractors for X rays and extreme ultraviolet: theory and predicted performance," Appl. Opt. **20**, 3027–3034 (1981).
9. E. Gullikson, C. Cerjan, D. Stearns, P. Mirkarimi, and D. Sweeney, "Practical approach for modeling extreme ultraviolet lithography mask defects," J. Vac. Sci. Technol. B **20**, 81–86 (2002).
10. S. George, P. Naulleau, F. Salmassi, I. Mochi, E. Gullikson, K. Goldberg, and E. Anderson, "Extreme ultraviolet mask substrate surface roughness effects on lithographic patterning," J. Vac. Sci. Technol. B **28**, C6E23 (2010).
11. J. C. Stover, *Optical Scattering, Measurement and Analysis*, 2nd ed. (SPIE Optical Engineering, 1995).
12. J. W. Goodman, *Statistical Optics* (Wiley, 1985), Chap. 7, pp. 286–360.
13. P. Naulleau and S. George, "Validity of the thin mask approximation in extreme ultraviolet mask roughness simulations," Appl. Opt. **50**, 3346–3350 (2011).
14. P. Naulleau, I. Mochi, and K. Goldberg, "Optical modeling of Fresnel zoneplate microscopes," Appl. Opt. **50**, 3678–3684 (2011).